

CHARACTERISTIC QSO ACCRETION DISK TEMPERATURES FROM SPECTROSCOPIC CONTINUUM VARIABILITY

NICOLAS A. PEREYRA,¹ DANIEL E. VANDEN BERK,² DAVID A. TURNSHEK, AND D. JOHN HILLIER
University of Pittsburgh, Department of Physics and Astronomy, 3941 O'Hara Street, Pittsburgh, PA 15260; pereyra@prism-cs.com,
danvb@astro.psu.edu, turnshek@quasar.phyast.pitt.edu, jdjh@galah.phyast.pitt.edu

BRIAN C. WILHITE
University of Illinois, Department of Astronomy, 1002 West Green Street, Urbana, IL 61801; wilhite@astro.uiuc.edu

RICHARD G. KRON
University of Chicago, Department of Astronomy and Astrophysics, 5640 South Ellis Avenue, Chicago, IL 60637; rich@oddjib.uchicago.edu

DONALD P. SCHNEIDER
Pennsylvania State University, Department of Astronomy and Astrophysics, 504 Davey Laboratory, University Park, PA 16802;
dps@astro.psu.edu

AND

JONATHAN BRINKMANN
Apache Point Observatory, 2001 Apache Point Road, Post Office Box 59, Sunspot, NM 88349-0059; brinkmann@nmsu.edu

Received 2005 June 1; accepted 2005 December 28

ABSTRACT

Using Sloan Digital Sky Survey (SDSS) QSO spectra taken at multiple epochs, we find that the composite flux differences in the rest-frame wavelength range 1300–6000 Å can be fit by a standard thermal accretion disk model in which the accretion rate has changed from one epoch to the next (without considering additional continuum emission components). The fit to the composite residual has two free parameters: a normalizing constant and the average characteristic temperature \bar{T}^* . In turn, in a standard disk the characteristic temperature is dependent on the ratio of the mass accretion rate to the square of the black hole mass. Therefore, provided enough time has elapsed for a composite disk spectrum to adjust to a new average characteristic temperature, reasonably consistent with the standard model, we conclude that most of the UV-optical variability observed in QSOs may be due to processes involving changes in disk accretion rates. This is consistent with the conclusion that a significant fraction of a QSO's UV-optical spectrum comes directly from the disk.

Subject headings: accretion, accretion disks — quasars: general — ultraviolet: general

1. INTRODUCTION

It has long been suspected that QSOs are powered by matter accreting from a disk onto a supermassive black hole (e.g., Lin & Papaloizou 1996; Ulrich et al. 1997; Mirabel & Rodríguez 1999, and references therein). Also, a QSO is typically observed to present a “flattened” UV-optical spectrum or a “big blue bump” (e.g., Shields 1978; Malkan & Sargent 1982; Camenzind & Courvoisier 1984; Elvis et al. 1994; Czerny et al. 2003). In turn, the big blue bump has generally been interpreted as thermal disk emission (e.g., Elvis et al. 1986; Laor & Netzer 1989; Sanders et al. 1989; Fiore et al. 1995; Gu et al. 2001; Shalyapin et al. 2002). The standard model is a geometrically thin disk with local thermal emission based on conservation of energy and angular momentum (Shakura & Sunyaev 1973). The integrated standard disk model continuum presents a “flattened” spectrum due to the contribution of different disk surface temperatures at different radii. Reasonable agreements are found with the standard disk model and the UV-optical continua of QSOs (e.g., Malkan 1983; Czerny & Elvis 1987; Wandel & Petrosian 1988; Sun & Malkan 1989; Laor 1990; Krolik et al. 1991; Natali et al. 1998).

However, accretion disk continuum fits to the UV-optical spectra of QSOs typically require additional components such as the extrapolation of the X-ray continuum into the UV-optical, the extrapolation of the infrared continuum, and the inclusion of a “small blue bump” component near 3000 Å (e.g., Malkan 1983; Czerny & Elvis 1987; Wandel & Petrosian 1988; Sun & Malkan 1989; Laor 1990). Also, host galaxy light can contaminate the QSO spectrum at optical and longer wavelengths.

In this work, we study the average residual UV-optical continuum (continuum difference) of QSOs when they vary from their “faint” phases to their “bright” phases, rather than the continua at either phase. Wilhite et al. (2005) found that the emission lines vary relatively weakly with respect to continuum variations; the residual flux is dominated by continuum changes. By analyzing a composite residual spectrum, we find that the average UV-optical flux difference is approximately the same as that inferred from a standard accretion disk that has changed its mass accretion rate. Of course, this scenario is reasonable only if enough time has elapsed for the disk to adjust to a change in accretion rate. The composite residual is constructed from hundreds of QSOs observed by the Sloan Digital Sky Survey (SDSS; Wilhite et al. 2005). This study of the residual flux assumes that the UV-optical variability is due to only the disk itself, thus no additional emission components are considered when analyzing the residual. The advantage of this approach is that nonvariable emission sources that contribute to the continua do not contribute to the composite residual.

¹ Current address: Prism Computational Sciences, Inc., 455 Science Drive, Suite 140, Madison, WI 53711.

² Current address: Pennsylvania State University, Department of Astronomy and Astrophysics, 525 Davey Lab, University Park, PA 16802.

We are currently studying individual QSO spectra taken from the SDSS. If the continuum UV-optical variability in individual objects can also be accounted for by a standard accretion disk at rest-frame wavelengths longer than Ly α 1215 Å emission, then this may also lead to a method to probe the inner disk region by analyzing the difference between EUV³ rest-frame residual spectra and disk model predictions. The strongest flux for a disk under typical QSO parameters would occur in the EUV, and this emission would be produced in the inner disk region. In turn, the strongest deviations of a real disk from the standard disk model are expected to occur in the inner disk region due to radiative transfer effects (including X-ray irradiation) (e.g., Hubeny et al. 2001) and departures of the gravitational force from the standard Newtonian r^{-2} law (e.g., Frank et al. 1992; Krolik 1999). Figure 7.3 of Krolik (1999) shows the general relativistic reduction factors.

In § 2 we briefly discuss the emission distribution from a standard disk and present general relationships. We present the form in which the average characteristic disk temperature \bar{T}^* is calculated by analyzing the residual spectrum in § 3. In § 4 we apply the discussions of the previous two sections to a composite spectrum constructed from SDSS data. Summary and conclusions are presented in § 5.

2. STANDARD DISK MODEL

2.1. General Comments

We assume in this paper that any observed variability in a QSO's UV-optical continuum is solely due to a change in its accretion disk, and that a change in the accretion disk is due to a change in the disk's mass accretion rate (but see § 2.3). We also assume that the radial emission of the disk follows that of the standard disk model.

It is obvious that the standard disk model is an idealization, just as the assumption of blackbody emission is an idealization for the continua of stellar spectra. However, we choose to apply the standard model to this variability analysis for three reasons. First, the standard disk model includes much of the physics of an accretion disk, such as gravity from a large central mass determining the average velocity fields in the disk, angular momentum transport, conversion of gravitational energy to radiative emission (where in the standard model it is assumed to be locally blackbody), and a monotonic increase in temperature with decreasing radius (except at radii close to the inner disk radius). Local blackbody emission is a reasonable first approximation that accounts for the relatively “flat” continua observed in systems in which accretion disks are inferred.

Second, the radial emission distribution of the standard model is independent of the vertical disk structure and the details that generate viscosity within the disk; thus, in the study of continuum variability, the standard model can be reduced to the dependence on only two basic physical parameters, namely: the central black hole mass M_{bh} and the disk mass accretion rate \dot{M}_{accr} .

Third, it may be premature to use the more detailed, albeit more realistic, models of the disk continuum developed after Shakura & Sunyaev (1973) (e.g., Czerny & Elvis 1987; Wandel & Petrosian 1988; Sun & Malkan 1989; Laor 1990; Ross et al. 1992; Coleman & Shields 1993; Shields & Coleman 1994; Störzer et al. 1994; Dörrer et al. 1996; Hubeny et al. 2000, 2001). They generally do not present significant differences with the continuum of the standard model at wavelengths greater than ~ 3600 Å, but there

are strong differences at wavelengths $\lesssim 1300$ Å (see Fig. 13 in Hubeny et al. 2001). Since we are analyzing rest wavelength ranges >1300 Å, the conclusions of this work will not be significantly affected by discrepancies in the region containing the strongest predicted differences ($\lambda < 1300$ Å). For the 1300–3600 Å regime we note that Hubeny et al. (2000, 2001) discuss some of the predictions of more realistic models near the Balmer edge, effects due to the inclusion of heavy elements, and anisotropy in spectral shape due to viewing angle. Thus, after applying the standard model in this analysis, as opposed to a more detailed one, it will be of some interest to compare standard model predictions to observed composite spectrum residuals in the 1300–3600 Å range.

To extend the above point even further, we note that more detailed models clearly show that radiative transfer effects (that must be present) can generate significant changes in the disk continuum in the EUV. Therefore, if the analysis presented here continues to hold up for individual objects, and if it can be demonstrated that the residual spectrum of a QSO in a high versus low state is due to a change in accretion rate, it may be possible to study the emission contribution and structure of the inner disk region by analyzing the deviations in EUV variability between the standard model, more advanced models, and actual observations.

2.2. Radial Emission Distribution

The radial emission distribution of the standard accretion disk model (Shakura & Sunyaev 1973) is based on the following nine assumptions: (1) the disk is steady; (2) it is azimuthally symmetric; (3) the gravitational field is Newtonian; (4) the mass of the disk is negligible compared to that of the black hole; (5) the mass within the disk follows Keplerian orbits; (6) conservation of angular momentum holds as shear stresses cause the disk mass to spiral inwards; (7) the shear stress in the disk at the innermost radius is zero; (8) conservation of energy holds as the loss of gravitational energy is converted into radiation; and (9) the disk surface emission is locally blackbody. We also make the additional assumptions that the outer disk radius is much larger than the inner disk radius and, as was done by Shakura & Sunyaev (1973), that the innermost disk radius is given by the last stable circular orbit as determined by general relativity (GR) under a Schwarzschild metric.

Thus, one finds (e.g., see Frank et al. 1992) that the luminosity of the standard disk is

$$F_{\lambda} = \left(\frac{6G}{c^2}\right)^2 M_{\text{bh}}^2 \int_1^{\infty} \pi \frac{2hc^2/\lambda^5}{\exp\{hc/[\lambda kT^*(s)]\} - 1} 4\pi s ds, \quad (1)$$

where G is the gravitational constant, c is the speed of light, M_{bh} is the black hole mass, h is Planck's constant, k is Boltzmann's constant, s is the radius divided by the innermost disk radius, the function $t(s) \equiv [s^{-3}(1 - s^{-1/2})]^{1/4}$, and the expression for the characteristic temperature is

$$T^* \equiv \left(\frac{\dot{M}_{\text{accr}} c^6}{576\pi G^2 M_{\text{bh}}^2 \sigma_S}\right)^{1/4}, \quad (2)$$

where \dot{M}_{accr} is the mass accretion rate and σ_S is the Stefan-Boltzmann constant. From the results of this standard disk formalism it can be seen that the continuum shape of a standard disk with black hole mass M_{bh} depends on only one physical parameter, the characteristic temperature T^* .

³ In this paper EUV refers to the wavelength range 200–912 Å.

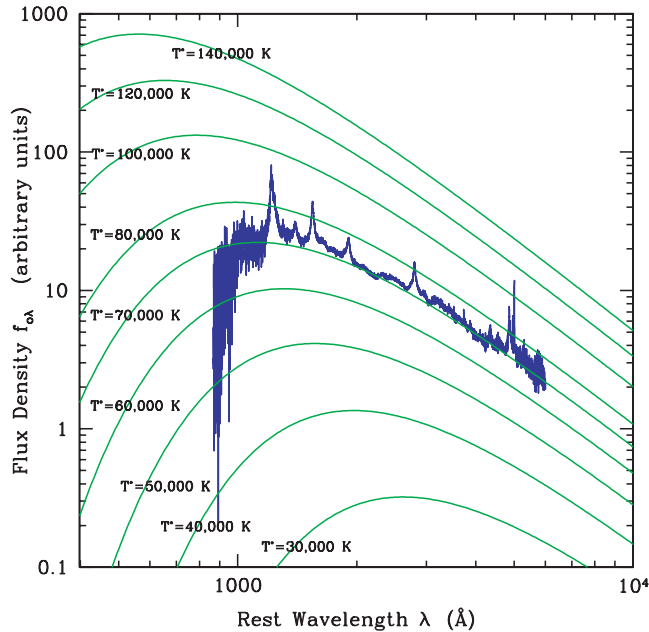


FIG. 1.—Flux of an SDSS QSO composite spectrum (blue) in arbitrary units vs. rest wavelength in Å, superimposed with the luminosity of a standard disk with different characteristic temperatures T^* (green) in arbitrary units. The disk mass accretion rate \dot{M}_{accr} is proportional to $(T^*)^4$ (eq. [2]). This plot illustrates that the UV-optical continuum of QSOs is qualitatively consistent with thermal emission from an accretion disk. Also, different T^* values lead to changes in the shape of the disk continuum spectrum. The composite spectrum was constructed using single-epoch spectra (no QSO contributing more than one spectrum) from the SDSS Data Release 1 QSO catalog, regardless of the variability properties.

2.3. Qualitative Comparison with Observations

As discussed in § 1, different authors have noted that the “flattened” UV-optical spectra observed in QSOs are qualitatively consistent with disk models. To illustrate this point, we show in Figure 1 the luminosity calculated using equation (1) for different disk mass accretion rates superimposed with a QSO composite constructed from SDSS data by Wilhite et al. (2005). In Figure 1 it can be seen that changes in the mass accretion rate \dot{M}_{accr} produce changes in the form of the disk continuum spectrum. The intent of this study is to use residual spectra (i.e., the difference between two spectra observed at different epochs) to make comparisons with disk models. Thus, one further assumption of this work is that there is sufficient time between mean observation epochs to permit us to model the change in brightness with a change in mass accretion rate \dot{M}_{accr} . That is, there is the implicit assumption that enough time has elapsed between the bright and faint phases of the composite QSO spectra for the accretion disks to adjust to a new characteristic average temperature that is reasonably well approximated by the standard model. The degree to which this assumption may hold is unclear. See, for example, Pringle (1981), Krolik (1999), and Webb & Malkan (2000) for some discussion on timescales.

The majority of AGNs present continuum variability on the order of 10% on timescales of months to years (Sirola et al. 1998; Vanden Berk et al. 2004). It is notable that these timescales are roughly consistent with estimated sound-speed timescales for accretion disks in AGNs. Sound-speed timescales measure the time it takes a density and pressure perturbation (i.e., a sound wave) to travel over a significant portion of the disk; such a perturbation would originate, for example, if there was a change in

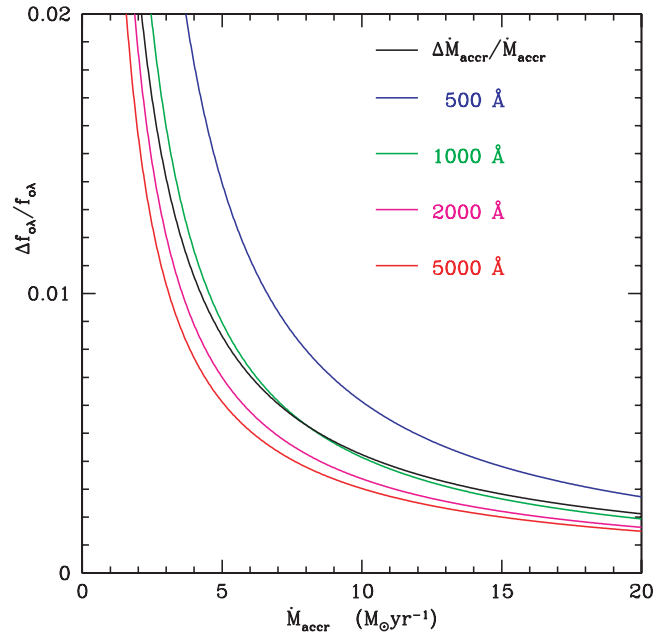


FIG. 2.—Relative change in flux of a standard disk vs. mass accretion rate for different wavelengths. The value of black hole mass used is $M_{\text{bh}} = 10^9 M_{\odot}$. The change in mass accretion rate is assumed constant ($\Delta\dot{M}_{\text{accr}} = 0.04 M_{\odot} \text{ yr}^{-1}$). This figure shows that, within typical QSO parameters, the continuum spectrum of a standard disk becomes bluer as its mass accretion rate increases (or equivalently, as its luminosity increases). This is consistent with observations of UV-optical variability in QSOs, in that, as discussed in the text, the QSO UV-optical continuum typically becomes bluer as it becomes brighter.

mass accretion rate.⁴ For the standard model the radiative emission depends directly on the mass accretion rate (eqs. [1] and [2]). When adjusting to a change in accretion rate, the disk would have to reestablish some degree of thermal balance. The thermal timescale, given by the ratio of the disk thermal content to its heating rate, is inversely proportional to the viscosity, which is largely unknown. The upper limit on the time it takes a disk to adjust to an accretion rate variation would involve the inflow timescale, so this may also be relevant. The inflow timescale is characteristically a factor of $(r/h)^2$ larger than the thermal timescale, where r is disk radius and h is disk thickness. Thus, given the current understanding of AGN accretion disk models, it is not straight forward to evaluate the assumption that enough time has elapsed for the disk to adjust to a new standard disk with a different characteristic temperature. Indeed, the results of this work, which we show are empirically consistent with interpreting the change in composite brightness as a change in accretion rate (§ 4), may also be revealing important clues about the geometry and (especially low) viscosity of AGN accretion disks. In fact, some investigators (e.g., Siemiginowska & Czerny 1989; Starling et al. 2004) have used observed brightness variations to infer constraints on accretion disk viscosity.

Figure 2 shows the relative change in flux of a standard disk versus mass accretion rate for different wavelengths for our

⁴ The total pressure is equal to the sum of gas pressure and radiation pressure. For a standard disk with typical AGN parameters, the disk height in the inner disk region is determined by radiation pressure (rather than gas pressure). This implies that if one estimates the sound speed solely taking into account gas pressure (i.e., taking radiation pressure to be zero), one significantly underestimates the sound speed in the inner disk region, and thus significantly overestimates the sound-speed timescales.

model. The value of black hole mass used is $M_{\text{bh}} = 10^9 M_{\odot}$. The change in mass accretion rate is assumed constant ($\Delta M_{\text{accr}} = 0.04 M_{\odot} \text{ yr}^{-1}$). Figure 2 shows that, within typical QSO parameters, the continuum spectrum of a standard disk becomes bluer as its mass accretion rate increases (or equivalently, as its luminosity increases). This is qualitatively consistent with observations that show that the optical-UV continua of QSOs are generally bluer in more luminous phases (e.g., Cutri et al. 1985; Edelson et al. 1990; Kinney et al. 1991; Paltani & Courvoisier 1994; Webb & Malkan 2000; Vanden Berk et al. 2004; Wilhite et al. 2005).

3. DETERMINATION OF \bar{T}^* FROM THE RESIDUAL SPECTRUM

3.1. General Comments

In performing fits to the residual spectrum, we assume that the shape of the disk flux continuum is isotropic (projection effects will introduce a viewing angle dependence to the observed disk flux, but independent of wavelength), and thus the observed disk flux would be equal to the luminosity up to a normalizing constant. Relativistic effects will introduce dependence of the continuum shape on viewing angle (e.g., special relativistic beaming and GR light bending). Radiative transfer effects (e.g., limb darkening) will also introduce dependence of the continuum shape on viewing angle; however, disk atmosphere models suggest that for wavelength ranges above $\sim 3600 \text{ \AA}$ significant changes in the continuum shape will occur only at high viewing angles (close to edge-on). The strongest changes for wavelengths between ~ 1300 and $\sim 3600 \text{ \AA}$ will also occur at high viewing angles (see Fig. 12 in Hubeny et al. 2000), and that would include only a fraction of objects assuming a random disk orientation in the QSO population.

3.2. Determination of the Average Characteristic Disk Temperature \bar{T}^*

To simplify the expressions, we define

$$g_{\lambda}(T^*) \equiv \int_1^{\infty} \pi \frac{2hc^2/\lambda^5}{\exp\{hc/[\lambda kT^*t(s)]\} - 1} 4\pi s ds. \quad (3)$$

The observed disk flux $f_{o,\lambda}$ will be proportional to the disk luminosity (eq. [1]). Therefore,

$$f_{o,\lambda} = c_o g_{\lambda}(T^*), \quad (4)$$

where c_o is a constant that depends on the black hole mass (see eq. [1], the object's cosmological distance, and the disk viewing angle (as a consequence of the projected area of the disk).

In this work, we assume that between the two epochs, the disk evolves from one steady state to another steady state with a change in mass accretion rate $\Delta \dot{M}_{\text{accr}}$. Since the black hole mass would not change significantly on the timescales considered here, it follows that the normalizing factor c_o remains constant, but the characteristic disk temperature T^* will vary (eq. [2]). Therefore, the residual spectrum $\Delta f_{o,\lambda}$ is given by

$$\begin{aligned} \Delta f_{o,\lambda} &= f_{2,o,\lambda} - f_{1,o,\lambda} \\ &= c_o g_{\lambda}(T_2^*) - c_o g_{\lambda}(T_1^*) = c_o [g_{\lambda}(T_2^*) - g_{\lambda}(T_1^*)] \end{aligned} \quad (5)$$

where the subindexes 1 and 2 correspond to each epoch.

Considering a Taylor series about the average characteristic temperature

$$\bar{T}^* \equiv \frac{1}{2}(T_2^* + T_1^*), \quad (6)$$

and defining

$$\Delta T^* \equiv T_2^* - T_1^*, \quad (7)$$

we have

$$\begin{aligned} g_{\lambda}(T_2^*) &= g_{\lambda}(\bar{T}^*) + \left(\frac{\Delta T^*}{2}\right) \left. \frac{\partial g_{\lambda}}{\partial T^*} \right|_{\bar{T}^*} + \frac{1}{2} \left(\frac{\Delta T^*}{2}\right)^2 \left. \frac{\partial^2 g_{\lambda}}{\partial T^{*2}} \right|_{\bar{T}^*} \\ &\quad + \frac{1}{6} \left(\frac{\Delta T^*}{2}\right)^3 \left. \frac{\partial^3 g_{\lambda}}{\partial T^{*3}} \right|_{\bar{T}^*} + \dots \end{aligned} \quad (8)$$

and

$$\begin{aligned} g_{\lambda}(T_1^*) &= g_{\lambda}(\bar{T}^*) - \left(\frac{\Delta T^*}{2}\right) \left. \frac{\partial g_{\lambda}}{\partial T^*} \right|_{\bar{T}^*} + \frac{1}{2} \left(\frac{\Delta T^*}{2}\right)^2 \left. \frac{\partial^2 g_{\lambda}}{\partial T^{*2}} \right|_{\bar{T}^*} \\ &\quad - \frac{1}{6} \left(\frac{\Delta T^*}{2}\right)^3 \left. \frac{\partial^3 g_{\lambda}}{\partial T^{*3}} \right|_{\bar{T}^*} + \dots \end{aligned} \quad (9)$$

It follows that

$$g_{\lambda}(T_2^*) - g_{\lambda}(T_1^*) = \Delta T^* \left. \frac{\partial g_{\lambda}}{\partial T^*} \right|_{\bar{T}^*} + \frac{1}{3} \left(\frac{\Delta T^*}{2}\right)^3 \left. \frac{\partial^3 g_{\lambda}}{\partial T^{*3}} \right|_{\bar{T}^*} + \dots \quad (10)$$

Therefore, considering equation (5), the residual spectrum $\Delta f_{o,\lambda}$ is given by

$$\Delta f_{o,\lambda} = c_o \Delta T^* \left. \frac{\partial g_{\lambda}}{\partial T^*} \right|_{\bar{T}^*} + \frac{c_o}{3} \left(\frac{\Delta T^*}{2}\right)^3 \left. \frac{\partial^3 g_{\lambda}}{\partial T^{*3}} \right|_{\bar{T}^*} + \dots \quad (11)$$

In this work, to simplify the analysis, we introduce the following approximation:

$$\Delta f_{o,\lambda} \approx c_o \Delta T^* \left. \frac{\partial g_{\lambda}}{\partial T^*} \right|_{\bar{T}^*}. \quad (12)$$

The function g_{λ} (eq. [3]) depends on only one independent physical parameter, the characteristic temperature T^* . Therefore, the process of fitting the residual spectra is reduced to the determination of two parameters: the product $c_o \Delta T^*$ and the average characteristic temperature \bar{T}^* .

We determine these two parameters by the standard method of maximum likelihood under the assumption of Gaussian flux error distributions. That is, we determine the values of the two free parameters, $c_o \Delta T^*$ and \bar{T}^* , that minimize

$$\chi^2 \equiv \sum_i \frac{1}{\sigma_i^2} \left[\Delta f_{o,\lambda,i} - (c_o \Delta T^*) \left. \frac{\partial g_{\lambda,i}}{\partial T^*} \right|_{\bar{T}^*} \right]^2, \quad (13)$$

where σ_i is the error on the measurement of flux variation at wavelength λ_i . The standard deviation on the values of each of the two free parameters is calculated assuming, once again, standard Gaussian distributions.

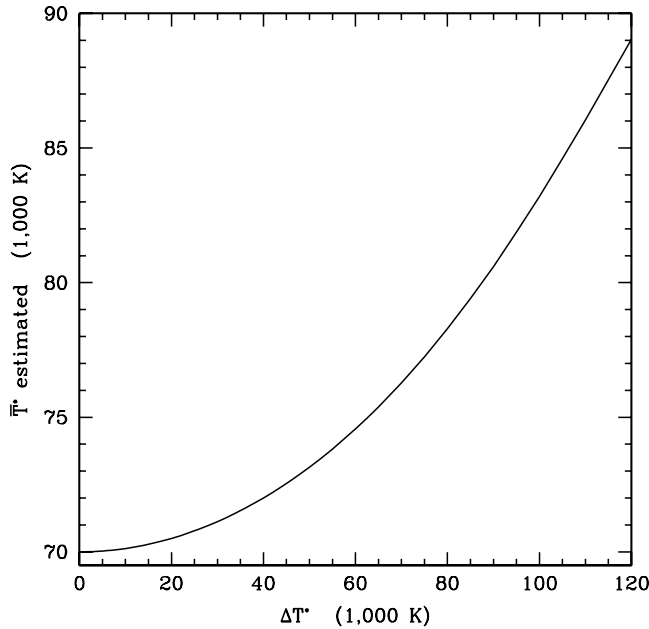


FIG. 3.— \bar{T}^* estimated through the method discussed in § 3.2 for “simulated” data between rest-frame wavelengths of 1300 and 6000 Å, that is, for simulated data representing the exact residual flux from the standard disk model (§ 2). The exact value of \bar{T}^* is 70,000 K, and a measurement error of 5% on the simulated flux measurements of the bright and faint phase is assumed. For the above parameters, accurate values for \bar{T}^* are obtained for variations in temperature of up to $\Delta T \approx 15,000$ K. That is, the method estimates accurate values for \bar{T}^* (for the parameters used here) for changes in mass accretion rate \dot{M}_{accr} of up to approximately a factor of 2 (see eq. [2]). The reason that the characteristic temperature \bar{T}^* becomes overestimated for larger variations in temperature ΔT^* , is that the third and higher order terms of eq. (11) are no longer negligible.

We wish to note at this point that our first attempt to determine characteristic disk temperature was based on minimizing $\chi^2 = \sum_i \{ \Delta f_{o,\lambda,i} - c_o [g_{\lambda i}(T_{\text{bright}}^*) - g_{\lambda i}(T_{\text{faint}}^*)] \}^2 / \sigma_i^2$ (rather than minimizing eq. [13]), and this in turn implied determining the three free parameters c_o , T_{bright}^* , and T_{faint}^* (rather than the two free parameters $c_o \Delta T^*$ and T^*). One obvious potential advantage of this alternative method is that in principle it can be applicable for an arbitrarily large temperature difference $\Delta T^* = T_{\text{bright}}^* - T_{\text{faint}}^*$. However, when we applied the method to actual data we found that there were several pairs of $(T_{\text{bright}}^*, T_{\text{faint}}^*)$ that produced local minima in the corresponding χ^2 . On further analysis we found that the different determined pairs $(T_{\text{bright}}^*, T_{\text{faint}}^*)$ had the same average characteristic temperature $\bar{T}^* = (T_{\text{bright}}^* + T_{\text{faint}}^*)/2$. This clearly suggested that the \bar{T}^* was, at least in our initial test cases, better constrained than either T_{bright}^* or T_{faint}^* . This specific result can be understood in terms of the standard disk model when ΔT^* is relatively small, as can be seen from equation (11) if the higher order terms of the expansion on the right hand side are negligible. Developing a fitting method based on \bar{T}^* lead us to the method we present here.

3.3. Testing the Method Against “Simulated” Data

In order to test the ability of the method described in § 3.2 to determine correct values of \bar{T}^* ,⁵ we apply it to “simulated” data in which the *exact* value of \bar{T}^* is previously known.

For the test data, we have fixed the value $\bar{T}^* = 70,000$ K (which corresponds to typical QSO parameters: $M_{\text{bh}} = 10^9 M_{\odot}$, $\dot{M}_{\text{accr}} \approx 1 M_{\odot} \text{ yr}^{-1}$), and have varied the value of ΔT^* for the

⁵ Assuming of course that a reasonable value for χ^2/n is found, where n is the degrees of freedom; i.e., $n = \text{number of data points} - \text{number of free parameters}$.

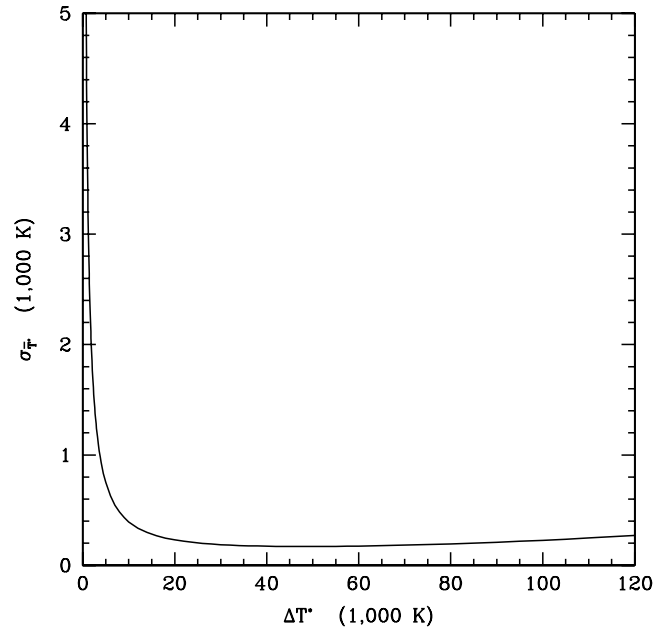


FIG. 4.—Standard deviation $\sigma_{\bar{T}^*}$ on the estimated value of \bar{T}^* obtained through the method discussed in § 3.2 for “simulated” data as described in and for the same physical parameters of Fig. 3. The exact value of \bar{T}^* is 70,000 K. For the above physical parameters, the standard deviation $\sigma_{\bar{T}^*}$ is less than 15,000 K for values of ΔT^* greater than ≈ 250 K. The value of $\sigma_{\bar{T}^*}$ becomes significantly large (i.e., comparable to the value of \bar{T}^*) at very low temperature variations ΔT^* because errors on the flux measurements of the bright and faint phases become larger than the residual flux.

assumed constant black hole mass of $M_{\text{bh}} = 10^9 M_{\odot}$. We have also assumed an error of 5% on measurement of flux at all wavelengths for both the “bright” and the “faint” epochs.

That is, we have calculated the luminosity for $T_2^* = \bar{T}^* + \Delta T^*/2$ from equation (1) for $\bar{T}^* = 70,000$ K, for the aforementioned value of black hole mass, for a discrete number of wavelengths between 1300 and 6000 Å, and taken these to be the measured data points for the bright phase with a measurement error of 5% on all points. Equivalently, we have also calculated the luminosity for $T_1^* = \bar{T}^* - \Delta T^*/2$ from equation (1) and taken these values to be the measured data points for the faint phase. The specific values used for the wavelengths λ_i are taken to be same as those obtained through the construction of the SDSS composite spectra that is studied in § 4.

In Figure 3, we show the estimated value \bar{T}^* versus the variation in temperature ΔT^* . For the above parameters, accurate values for \bar{T}^* are obtained for variations in temperature of up to $\Delta T \approx 15,000$ K. That is, the method estimates accurate values for \bar{T}^* (for the parameters used here) for changes in mass accretion rate \dot{M}_{accr} of up to approximately a factor of 2 (see eq. [2]). The reason that the characteristic temperature \bar{T}^* becomes overestimated for larger variations in temperature ΔT^* (see Fig. 3), is that the third and greater order terms of equation (11) are no longer negligible.

In Figure 4, we show the standard deviation of the estimated value of \bar{T}^* , $\sigma_{\bar{T}^*}$, versus the variation in temperature ΔT^* . For the above physical parameters, the standard deviation $\sigma_{\bar{T}^*}$ is less than 15,000 K for values of ΔT^* greater than ≈ 250 K. The reason that $\sigma_{\bar{T}^*}$ becomes significantly large (i.e., comparable to the value of \bar{T}^*) at very low temperature variations ΔT^* , is that errors on the flux measurements of the bright and faint phases become larger than the residual flux.

Thus, we have shown that for a disk characteristic temperature of 70,000 K, if the UV-optical variability in QSOs is due to

changes in mass accretion rate \dot{M}_{accr} , then the method described in § 3.2 will be capable of accurately and effectively constraining the average disk characteristic temperature \bar{T}^* , as long as the temperature variation ΔT^* is greater than ≈ 250 K and the changes in mass accretion rate \dot{M}_{accr} are not significantly greater than about a factor of 2.

4. APPLICATION TO SDSS COMPOSITE SPECTRA

4.1. Construction of the Composite Residual Spectrum

The systematic construction of the composite residual spectrum from over 300 QSOs taken from the SDSS is discussed in detail in a separate paper (Wilhite et al. 2005). To avoid redundancy, we shall present here only a brief discussion of the construction of the composite, and focus rather on analyzing the composite residual within the assumption that it is generated by a change in mass accretion rate of a standard disk that evolves from one steady state to another, applying the methods discussed above.

The SDSS (see York et al. 2000; Stoughton et al. 2002, and references therein for a technical summary) is producing a large homogeneous sample of spectroscopically observed QSOs (Schneider et al. 2003). The QSOs are targeted (Blanton et al. 2003) according to the algorithm described by Richards et al. (2002) from photometric data in the SDSS imaging survey (Fukugita et al. 1996; Gunn et al. 1998; Hogg et al. 2001; Smith et al. 2002; Pier et al. 2003; Ivezić et al. 2004). Most of the QSOs used by Wilhite et al. (2005) are identified in the third SDSS data release (Abazajian et al. 2005). QSOs that were spectroscopically observed at least twice by the SDSS (see Fig. 5 for a rest-frame time lag histogram of the sample) were searched for clear evidence of variability in the observer frame optical (UV-optical QSO rest frame). Stars observed simultaneously with the QSOs were used to calibrate the observed fluxes (under the assumption that the stellar fluxes are constant), and to systematically establish the maximum variation in flux measurements that could be attributed to experimental noise.

As discussed by Wilhite et al. (2005), the redshift and absolute magnitude distributions of the variable and nonvariable QSO samples are indistinguishable. The median redshifts are $z = 1.47$ and 1.51 for the variable and nonvariable samples respectively, and the respective median absolute magnitudes are $M_r = -24.9$ and -25.2 .

A residual spectrum was calculated for each of the QSOs that were identified to have clearly presented a variation in its UV-optical rest-frame continuum. The individual rest-frame residual spectra were scaled to unity at a predefined wavelength (3060 Å). The composite residual (Fig. 6) was then constructed by averaging the individually scaled residual spectra.

Note that there was no selection of the sample with respect to the possible influence of dust characteristics. It is conceivable that the sample is biased in some way—having either more or less dust than other QSOs—but such a bias, if present, is not obvious, and this possibility was not investigated. Whether dust and variability are correlated in some way is beyond the scope of the present paper. However, the effect of dust extinction would be to redden the difference spectra, so our temperature estimates would be biased to lower values.

4.2. Fitting the Residual Spectrum

Following the methods discussed in § 3.2, we have fit the SDSS composite residual spectrum discussed in § 4.1. As discussed in § 3.2, the two free parameters of the fit are a constant scaling factor and the average disk characteristic temperature \bar{T}^* .

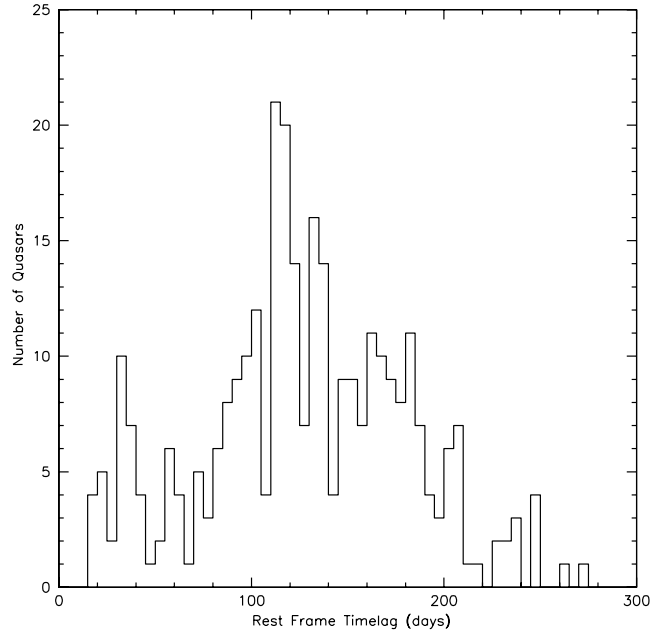


FIG. 5.—Rest-frame time lag histogram of the SDSS QSO object sample used in the construction of the composite residual spectrum. The median rest-frame time lag is 124.5 days, and the full sample ranges from 17.5 to 270.4 days.

As discussed by Wilhite et al. (2005), the strength of the emission line components in the residual are significantly reduced with respect to the line strengths in the spectra of either the bright or faint phases; this point is illustrated by comparing Figures 1 and 6. That is, relative to the continuum variations, the emission lines vary relatively weakly. However, residual features at the locations of some major emission lines are visible in the composite difference spectrum.

We calculate several different fits to the residual spectrum by using the whole data spectrum (800–6000 Å), by excluding wavelengths below 912 Å (i.e., below the Lyman limit), by excluding wavelengths below 1300 Å (to exclude flux contributions from the Ly α 1215 Å line and to avoid the Ly α forest absorption), and by excluding the contribution of other strong emission lines. The results are presented in Table 1. The second column gives the wavelength ranges used for the fits, the third column lists strong emission lines whose flux contributions are excluded from the fits (due to the wavelength ranges of the first column), the fourth column gives the derived average characteristic temperatures \bar{T}^* , the fifth column gives the derived uncertainties (2σ) on \bar{T}^* (calculated under the standard assumption of Gaussian distributions), and the sixth column gives the reduced chi-squared values χ^2/n (where n is the number of degrees of freedom [number of data points minus number of free parameters]).

In Figure 7, we present the composite QSO residual spectra derived from SDSS data excluding wavelengths lower than 1300 Å, and excluding wavelengths associated with the four emission lines indicated in the third column of the last row of Table 1, superimposed with the fit of a standard disk that has changed its mass accretion rate \dot{M}_{accr} . The average characteristic temperature of the fit is $\bar{T}^* = 92,700 \text{ K} \pm 700 \text{ K}$ and the value for the reduced χ^2 of the fit is $\chi^2/n = 2.993$ (see the last row of Table 1). Figure 7 shows that the composite residual spectrum is quantitatively consistent with the explanation that the residual is caused by the change of mass accretion rate \dot{M}_{accr} in a standard disk.

The best fit to the residual spectrum for a single-temperature blackbody fit is also shown in Figure 7. The blackbody fit with

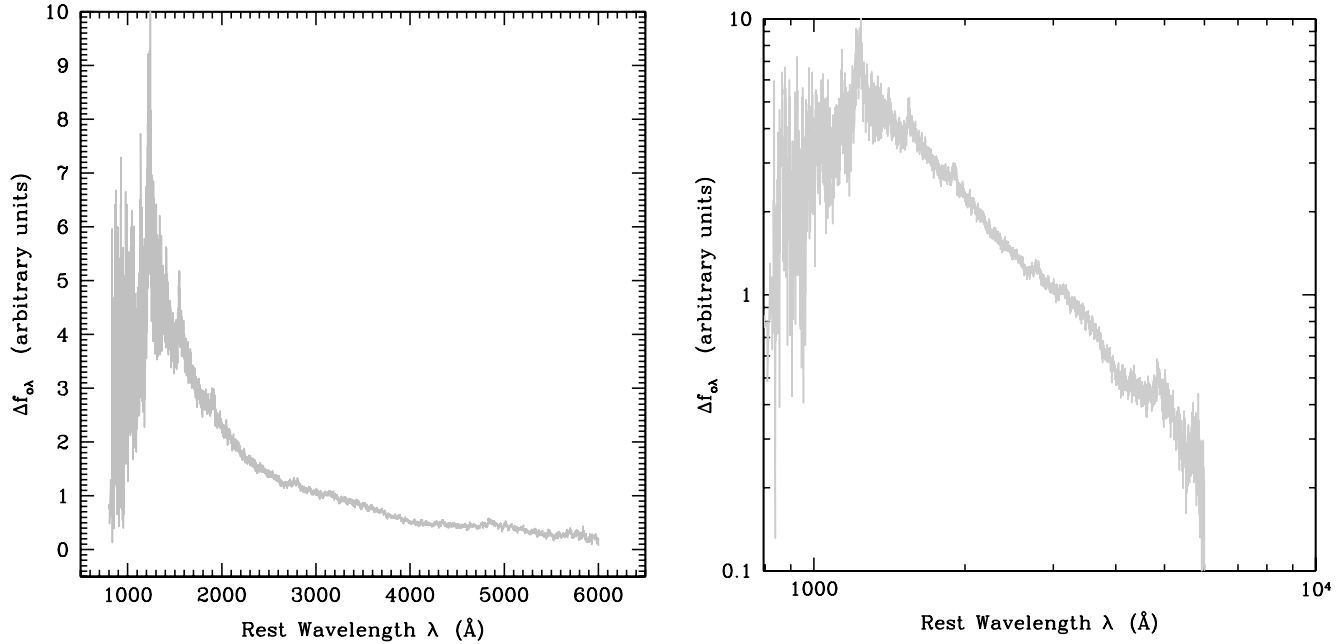


FIG. 6.—*Left*: Composite QSO residual spectrum derived from SDSS data. *Right*: Same plot in log-log scale. Details on the construction of the composite are presented in a separate paper (Wilhite et al. 2005). The flux of the residual spectrum tends to become larger at lower wavelengths. Although the strength of the emission lines is significantly reduced in the residual spectra, with respect to corresponding line strengths in the spectra of either the bright or faint phases (e.g., see Fig. 1), they are still detectable.

a temperature of 15,500 K is clearly quite poor. Models for which the difference spectrum might reasonably be described by a single blackbody, such as individual supernova explosions or localized hot spots, are not supported by the composite residual spectrum.

Almost all the data used here are different subsets of wavelengths above the Lyman limit (912 Å) of the QSO rest frame (Table 1). Below these wavelengths it is likely that deviations between the observations and the standard disk model will occur for several reasons. First, as discussed in § 1, deviations of a real

disk from the standard model are expected below the Lyman limit due to radiative transfer effects and due to the departure of the gravitational force from the standard Newtonian form in the inner disk region. Second, for higher redshifts QSOs, it is more likely that intervening neutral hydrogen systems will produce

TABLE 1
ACCRETION DISK FITS TO THE COMPOSITE RESIDUAL SPECTRUM

Fit	λ (Å)	Excluded Lines	\bar{T}^{*a} (K)	$2\sigma_{\bar{T}^*}$ (K)	χ^2/n^b
1.....	800–6000	...	80,100	400	4.892
2.....	912–6000	...	82,400	400	4.695
3.....	1300–6000	...	95,500	700	3.345
4.....	1300–1500	C IV 1549 Å
	1600–6000	...	91,500	700	3.111
5.....	1300–1500	C IV 1549 Å
	1600–2750	Mg II 2798 Å
	2850–6000	...	91,700	700	3.155
6.....	1300–1500	C IV 1549 Å
	1600–2750	Mg II 2798 Å
	2850–4810	H β 4861 Å
	4910–6000	...	92,700	700	2.965
7.....	1300–1500	C IV 1549 Å
	1600–2750	Mg II 2798 Å
	2850–4810	H β 4861 Å
	4910–5825,	He I 5875 Å
	5925–6000	...	92,700	700	2.993

^a The maximum disk surface temperature of a standard disk, T_{\max} , is approximately one-half of the characteristic temperature T^* (see § 2.2).

^b Reduced χ^2 , where n is the number of degrees of freedom.

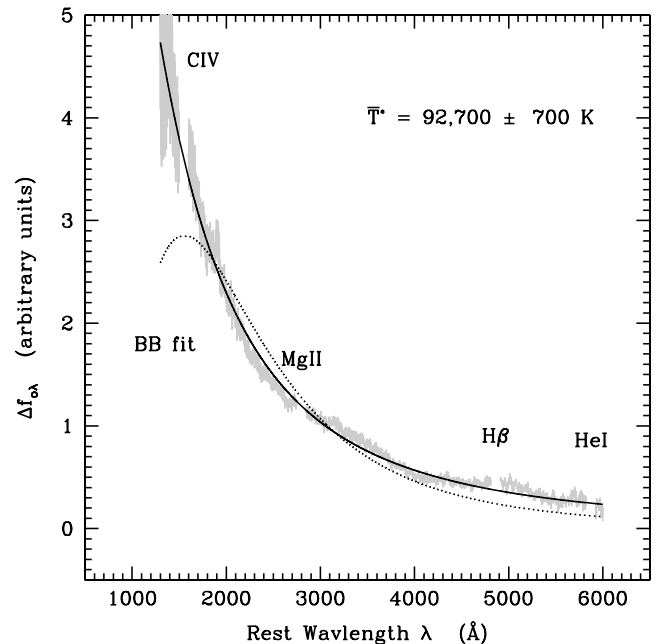


FIG. 7.—Composite QSO residual spectra derived from SDSS data, excluding wavelengths lower than 1300 Å and excluding wavelengths associated with the four emission lines indicated, superimposed with the fit of a disk (*solid curve*) that has changed its mass accretion rate \dot{M}_{accr} . The average characteristic temperature of the fit is $\bar{T}^* = 92,700 \pm 700$ K (see last row of Table 1). The maximum disk surface temperature T_{\max} is approximately one-half of the characteristic temperature T^* (see § 2.2). In addition, the best blackbody fit (*dotted curve*; $T_{\text{BB}} = 15,500$ K) to the composite residual is also shown.

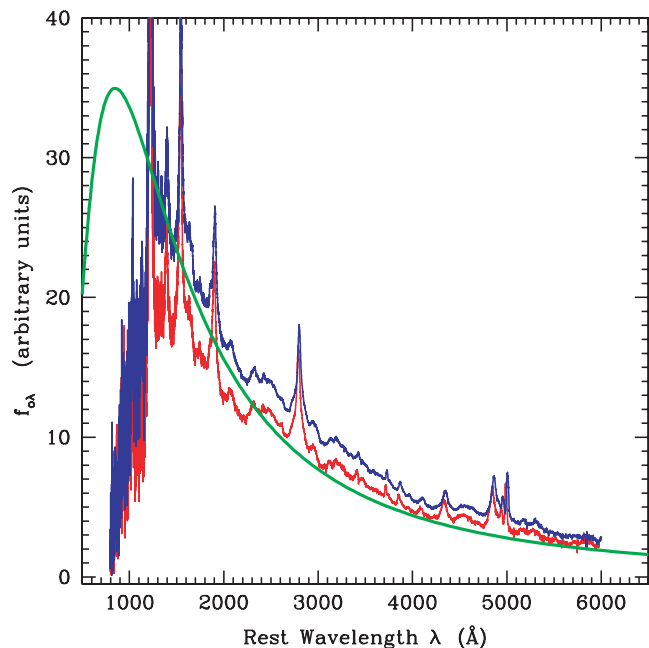


FIG. 8.—Bright SDSS QSO spectral composite (*blue*), faint SDSS QSO spectral composite (*red*), and the continuum of a standard disk (up to a normalizing constant) corresponding to a characteristic temperature of $T^* = 92,700$ K (*green*) (see Fig. 7). Although the standard disk model determines an excellent fit to the composite residual (Table 1, Fig. 7); when the fit is applied to the composite continuum (rather than to the residual), the disk continuum tends to underestimate the observed continuum around ~ 3000 Å (corresponding to the “small blue bump”) and to overestimate at shorter wavelengths.

significant absorption ($\text{Ly}\alpha$ forest) “occluding” of the disk continuum at wavelengths lower than the $\text{Ly}\alpha$ 1215 Å. A third reason is that other possibly variable components, such as a Compton upscattering component extending from X-ray wavelengths, which do not originate directly from the disk, will be important.

The average characteristic temperature that we derive from the composite residual spectra is thus *independent* of the continuum turnover that may or may not occur at $\lambda < \text{Ly}\alpha$. In fact, most of the fits are based on wavelengths above 1300 Å (Table 1; Fig. 7). The reason this is significant is that the characteristic temperature of the standard disk model is strongly dependent on the *actual* disk continuum turnover and in particular on the wavelengths at which this turnover occurs. Thus, if an observational continuum turnover is introduced at the Lyman limit due to radiative transfer effects at or near the disk or due to intervening absorption systems, rather than due to the radial distribution of disk photospheric emission, then attempts to fit the residual including data points below the Lyman limit would produce inconsistencies that could cause the disk characteristic temperature to be significantly underestimated.

This analysis has been applied only to a composite residual spectrum, and so it should give a reasonable value of T^* for typical QSOs. However, as we have not done this for individual QSOs, we do not know the distribution of T^* , nor its dependence on luminosity or other QSO parameters.

In Figure 8 we show the bright SDSS QSO spectral composite and the faint SDSS QSO spectral composite (Wilhite et al. 2005), superimposed with the continuum of a standard disk (up to a normalizing constant) corresponding to a characteristic temperature of $T^* = 92,700$ K. When the accretion disk fit is applied to

the composite continuum (rather than to the residual), while roughly reproducing the overall UV-optical continuum, it does not present such an excellent agreement with observations as it does with the composite residual (Fig. 7). Within the context of the models that are applied here, this is due to the contribution of non-variable sources that do not originate directly from the accretion disk. For example, the disk model continuum tends to underestimate the observed emission around ~ 3000 Å, corresponding to the “small blue bump” emission, which is probably composed mainly of Balmer continuum emission and Fe line complexes.

5. SUMMARY AND CONCLUSIONS

Under the assumption that the UV-optical variability in QSOs is due to a change of mass accretion rate in a standard disk, we have analyzed a composite QSO residual spectrum constructed from hundreds of objects observed by the SDSS. An advantage of using difference spectra is the ability to remove nonvariable components from the analysis. We have shown that our analysis technique can recover disk parameters in simulated data. The model is relatively simple—the shape of a difference spectrum depends only on the disk characteristic temperature T^* .

Our main conclusion is that, on average (i.e., through the SDSS composite), in the wavelength range 1300–6000 Å, residual QSO spectra can be quantitatively accounted for by a standard thermal disk that has varied from one steady state to another by changing its mass accretion rate. As emphasized in § 2.3, this result additionally relies on the assumption that a sufficient amount of time has elapsed between the mean epochs that characterize the high and low QSO states, such that the formalism developed here is valid.

Under our assumptions, these results suggest that UV-optical variability in QSOs is due to processes involving an accretion disk, and specifically that changes in mass accretion rates play a role. This is consistent with the idea that a significant fraction of the UV-optical spectrum comes directly from the disk, which has been suggested by many different authors.

We are currently studying individual QSO spectra taken from the SDSS. If the analysis shows consistency with individual objects, as it has done here for composite spectra, then we may have a method to probe the inner disk region by analyzing the difference between variable EUV and the standard disk model predictions. Also, if this method can be used with higher order terms, then there is a possibility of separating and determining black hole mass M_{bh} and disk mass accretion rate \dot{M}_{accr} , for direct comparison with other methods of measuring these parameters.

This work is supported in part by the National Science Foundation under grant AST 00-71193 and in part by the National Aeronautics and Space Administration under Grant ATP03-0104-0144. D. V. B. and D. P. S. were supported by National Science Foundation grant AST 03-07582. D. A. T. thanks Julian Krolik for discussions.

Funding for the creation and distribution of the SDSS Archive has been provided by the Alfred P. Sloan Foundation, the Participating Institutions, the National Aeronautics and Space Administration, the National Science Foundation, the U.S. Department of Energy, the Japanese Monbukagakusho, and the Max Planck Society. The SDSS Web site is <http://www.sdss.org>.

The SDSS is managed by the Astrophysical Research Consortium (ARC) for the Participating Institutions. The Participating

Institutions are the University of Chicago, Fermilab, the Institute for Advanced Study, the Japan Participation Group, Johns Hopkins University, the Korean Scientist Group, Los Alamos National Laboratory, the Max-Planck-Institute for Astronomy (MPIA), the

Max-Planck-Institute for Astrophysics (MPA), New Mexico State University, University of Pittsburgh, University of Portsmouth, Princeton University, the United States Naval Observatory, and the University of Washington.

REFERENCES

- Abazajian, K., et al. 2005, *AJ*, 129, 1755
 Blanton, M. R., Lin, H., Lupton, R. H., Maley, F. M., Young, N., Zehavi, I., & Loveday, J. 2003, *AJ*, 125, 2276
 Camenzind, M., & Courvoisier, T. J.-L. 1984, *A&A*, 140, 341
 Coleman, H. H., & Shields, G. A. 1993, *Rev. Mexicana Astron. Astrofis.*, 27, 95
 Cutri, R. M., Wiśniewski, W. Z., Rieke, G. H., & Lebofsky, M. J. 1985, *ApJ*, 296, 423
 Czerny, B., & Elvis, M. 1987, *ApJ*, 321, 305
 Czerny, B., Nikolajuk, M., Róžańska, A., Dumont, A.-M., Loska, Z., & Życki, P. T. 2003, *A&A*, 412, 317
 Dörrer, T., Riffert, H., Staubert, R., & Ruder, H. 1996, *A&A*, 311, 69
 Edelson, R. A., Krolik, J. H., & Pike, G. F. 1990, *ApJ*, 359, 86
 Elvis, M., Green, R. F., Bechtold, J., Schmidt, M., Neugebauer, G., Soifer, B. T., & Mathews, K. 1986, *ApJ*, 310, 291
 Elvis, M., et al. 1994, *ApJS*, 95, 1
 Fiore, F., Elvis, M., Siemiginowska, A., Wilkes, B. J., McDowell, J. C., & Mathur, S. 1995, *ApJ*, 449, 74
 Frank, J., King, A., & Raine, D. 1992, *Accretion Power in Astrophysics* (Cambridge: Cambridge Univ. Press)
 Fukugita, M., Ichikawa, T., Gunn, J. E., Doi, M., Shimasaku, K., & Schneider, D. P. 1996, *AJ*, 111, 1748
 Gu, M., Cao, X., Jiang, D. R., & Xu, Y. 2001, *MNRAS*, 321, 369
 Gunn, J. E., et al. 1998, *AJ*, 116, 3040
 Hogg, D. W., Finkbeiner, D. P., Schlegel, D. J., & Gunn, J. E. 2001, *AJ*, 122, 2129
 Hubeny, I., Agol, E., Blaes, O., & Krolik, J. H. 2000, *ApJ*, 533, 710
 Hubeny, I., Blaes, O., Krolik, J. H., & Agol, E. 2001, *ApJ*, 559, 680
 Ivezić, Z., et al. 2004, *Astron. Nachr.*, 325, 583
 Kinney, A. L., Bohlin, R. C., Blades, J. C., & York, D. G. 1991, *ApJS*, 75, 645
 Krolik, J. H. 1999, *Active Galactic Nuclei: From the Central Black Hole to the Galactic Environment* (Princeton: Princeton Univ. Press)
 Krolik, J. H., Home, K., Kallman, T. R., Malkan, M. A., & Edelson, R. A. 1991, *ApJ*, 371, 541
 Laor, A. 1990, *MNRAS*, 246, 369
 Laor, A., & Netzer, H. 1989, *MNRAS*, 238, 897
 Lin, D. N. C., & Papaloizou, J. C. B. 1996, *ARA&A*, 34, 703
 Malkan, M. A. 1983, *ApJ*, 268, 582
 Malkan, M., & Sargent, W. 1982, *ApJ*, 254, 22
 Mirabel, I. F., & Rodríguez, L. F. 1999, *ARA&A*, 37, 409
 Natali, F., Giallongo, E., Cristiani, S., & La Franca, F. 1998, *AJ*, 115, 397
 Paltani, S., & Courvoisier, T. J.-L. 1994, *A&A*, 291, 74
 Pier, J. R., Munn, J. A., Hindsley, R. B., Hennessy, G. S., Kent, S. M., Lupton, R. H., & Ivezić, Z. 2003, *AJ*, 125, 1559
 Pringle, J. E. 1981, *ARA&A*, 19, 137
 Richards, G. T., et al. 2002, *AJ*, 123, 2945
 Ross, R. R., Fabian, A. C., & Mineshige, S. 1992, *MNRAS*, 258, 189
 Sanders, D. B., Phinney, E. S., Neugebauer, G., Soifer, B. T., & Mathews, K. 1989, *ApJ*, 347, 29
 Schneider, D. P., et al. 2003, *AJ*, 126, 2579
 Shakura, N. I., & Sunyaev, R. A. 1973, *A&A*, 24, 337
 Shalyapin, V. N., Goicoechea, L. J., Alcalde, D., Mediavilla, E., Muñoz, J. A., & Gil-Merino, R. 2002, *ApJ*, 579, 127
 Shields, G. A. 1978, *Nature*, 272, 706
 Shields, G. A., & Coleman, H. H. 1994, in *NATO Advanced Research Workshop on Theory of Accretion Disks*, ed. W. Duschl et al. (Dordrecht: Kluwer), 223
 Siemiginowska, A., & Czerny, B. 1989, *MNRAS*, 239, 289
 Sirola, C. J., et al. 1998, *ApJ*, 495, 659
 Smith, J. A., et al. 2002, *AJ*, 123, 2121
 Starling, R., Siemiginowska, A., Uttley, P., & Soria, R. 2004, *MNRAS*, 347, 67
 Störzner, H., Hauschildt, P. H., & Allard, F. 1994, *ApJ*, 437, L91
 Stoughton, C., et al. 2002, *AJ*, 123, 485
 Sun, W.-H., & Malkan, M. A. 1989, *ApJ*, 346, 68
 Ulrich, M.-H., Maraschi, L., & Urry, C. M. 1997, *ARA&A*, 35, 445
 Vanden Berk, D. E., et al. 2004, *ApJ*, 601, 692
 Wandel, A., & Petrosian, V. 1988, *ApJ*, 329, L11
 Webb, W., & Malkan, M. 2000, *ApJ*, 540, 652
 Wilhite, B. C., Vanden Berk, D. E., Kron, R. G., Schneider, D. P., Pereyra, N. A., Brunner, R. J., Richards, G. T., & Brinkman, J. V. 2005, *ApJ*, 633, 638
 York, D. G., et al. 2000, *AJ*, 120, 1579